www.rericjournal.ait.ac.th

Computational Fluid Dynamic (CFD) Analysis of Propeller Turbine Runner Blades using various Blade Angles

Pribadyo Pribadyo*,[1], Hadiyanto Hadiyanto*, and Jamari Jamari[#]

ARTICLE INFO

Article history:
Received 22 January 2021
Received in revised form
08 May 2021
Accepted 19 May 2021

Keywords:
Blade angle
Hydropower energy
Propeller turbine
Runner blade
Simulation CFD

ABSTRACT

In this study, computational fluid dynamics (CFD) methods were adopted to predict the runner blade performance of the propeller turbine. The geometrical parameters and internal performance parameters, such as flowrate (0.08 – 0.2 m^3/s), and the turbine runner model based on the three different blade angles (i.e., 25 degrees, 30 degrees, and 35 degrees), were analyzed, using Fluent ver.18.2. CFD commercial code. The Reynolds Averaged Navier Stokes equation with the shear stress transport k-ω turbulence models used to simulate the unsteady model, to predict the turbine performances by investigating dimensionless parameters such as tip speed ratio (λ), power coefficient (Cp), torque (T), etc. The performance characteristics of the runner blade on CFD data were compared with the reference case to analyze the suitability of the blade angle in potential energy extraction. The analysis found that the interaction between the flowrate and blade angle affects the performance of the turbine. The performance efficiency of the runner blade had also consistently shown the characteristic trend of nonlinear increases to peak to an optimum value, before decreasing with increased blade angle. Results found that both the power coefficient and the efficiency were higher for the blade angle of 25 degrees than for the blade angles of 30 degrees and 35 degrees.

1. INTRODUCTION

Since climate change represents an important global issue, several countries have increased their support mechanisms towards renewable energy (wind energy, solar cells, geothermal, biomass and hydropower) [1]. Hydropower constitutes a green technology that is cheap, environmentally friendly, and vital for the future of sustainable energy [2], with approximately 16 percent of the world's electrical energy needs [3]. Hydropower plays a significant role in electricity production in more than 150 countries [4]. Canada, China, and the United States are countries with the largest hydroelectric capacity [5]. Apart from being more efficient, hydropower is a better renewable energy source than wind or solar energy [6]. It is the only source of regenerative power that can supply electricity on an industrial scale and at a competitive cost, compared to fossil fuel energy [7], and [8].

As an archipelago, Indonesia has a huge hydropower potential, extending from Sabang to Merauke, only 9.4 percent of which is exploited [9]. The low utilization of the available green energy potential is due to the high level of investment required, the site's geographical location, the lack of human resources to operate and maintain the existing factory system, and the limitations of current day conventional turbines [10]. The most commonly utilized turbine for low head potential is the Kaplan turbines, capable of operating at a range of 2-40 meters [11]. However, this type of turbine requires relatively complex canals or channels to regulate water flow before and after the turbine, to achieve optimal performance. Hence, small hydropower using propeller turbines, which can operate in low head conditions (mainly "run of river") is the right choice for this goal [12], with its ability to overcome obstacles not found in conventional turbine designs [13]. The axial flow propeller turbines for low head micro-hydropower in Indonesia have been studied [14]. This turbine is very simple and does not require flow control before and after the turbine [15]. The design of this turbine is compact, suitable for isolated rural areas [16], particularly in Indonesia. Nevertheless, attention to this from researchers and equipment manufacturers is still less. However, this turbine can prove to be an innovative, environmentally friendly, and cost-effective solution for producing energy [17], since it can be integrated into a decentralized, off-grid design for rural areas that have limited access to electricity [18].

The main aspect of the propeller turbine as a hydropower on the low head conditions is the turbine, which can produce electricity with the maximum power using the mechanics power (torque) delivered by the

*Doctoral Program of Environmental Science of Postgraduate Studies, Diponegoro University, Semarang, Indonesia.

[#]Department of Mechanical Engineering, Faculty of Engineering, Diponegoro University, Semarang, Indonesia.

[1]Corresponding author:
Email: pribadyo@utu.ac.id.

runner. At the low flow rate, the higher the propeller turns, the greater the power output. When the propeller rotation reaches its peak (stall), the power will start decreasing slowly [19]. Thus, it is important to understand the blade design for optimal turbine performance, leading to the best efficiency point (BEP) [20]. The runner blade is the main component in the propeller turbine, which directly converts the potential energy contained in water into torque at the turbine shaft. Some of the factors that affect propeller turbine performance are the blade angle, the number of blades, and the turbine diameters. For a cost-effective design, it is important to predict the hydraulic behaviour before application. The experimental approach is much more expensive and takes long. Using computational fluid dynamics (CFD), it is possible to gain significant insights, in particular into defining fluid flow in hydraulic turbines [21]; [22]; [23]. CFD has been widely used in the literature to analyse the aerodynamic performance of propeller turbines [24] [25]. This CFD is an important, cost-effective tool for estimating turbine performance in terms of optimal design, allowing a better understanding of phenomena of flow behaviour in the turbine for different flow conditions [26].

Studies related to turbine blades have been carried out through experiment and computation [27]. Other researchers have shown that the propeller shape can increase turbine efficiency by 73.9 percent [28]. Lwin Oo *et al.* designed 5-kW propeller turbines, and the runner consists of four-blade, a flow of 0.38 m^3/sec and a 2.2 meters head. The design of the runner blade profile was calculated using Microsoft Excel drawn by SolidWorks software. The calculated runner diameter was 0.310 meter, and the hub, 0.124 meters. Nishi *et al.* investigated the designs of the axial flow hydraulic turbine runners using CFD analysis and compared them to an experiment. As a result, the runners designed have significantly improved turbine efficiency by 0.768 percent. Another work by Djodikusumo *et al.* relates to the 3D modelling of a propeller turbine runner utilizing Autodesk Inventor. The resulting 3D models were then meshed and simulated by using CFD software. CFD simulation results showed that hydraulic efficiency is only about 84-85%. Although the numerical and experimental studies have shown that turbines can work with the performance of goods in their application [32] [33], the authors hope to learn the application and excellence of these types of turbines based on the potential of existing energy sources in Indonesia. For analytical purposes, this specific turbine design, developed with pitch angles variations of 25 degrees, 30 degrees, and 35 degrees, has not been studied in depth by past researchers.

The objective of this study is to predict the runner blade performance of propeller turbines for operating conditions characterized by the flowrate range of 0.08 - 0.2 m^3/s. The hub and tip diameters are 0.06 meters and 0.30 meters respectively, and the runner of the blade consists of a four-blade.

2. METHODOLOGY

2.1 Blade Desain

The main focus of this study is the runner blade of the propeller turbine's curved shapes, which was chosen because it is more efficient [34]. The fundamental dimensions of the turbine can be easily estimated, once the specific speed is known. A large number of statistical studies on a numerous schemes have established a correlation of the specific speed and the net head for each type of turbine [11].

$$n_s = \frac{2.716}{H_n^{0.5}} \text{ (USBR).} \tag{1}$$

Using the specific speed n_s, obtained from (1), thus, the circumferential velocity coefficient k_u, hub ratio v, and the axial velocity coefficient k_a ar e calculated. In addition, the circumferential velocity u_t of a tip, the outer diameter D_e of a runner, and the hub diameter D_i are obtained with the following formulae:

$$\begin{aligned} u_t &= k_u\sqrt{2gH}, \\ D_i &= \frac{60u_t}{\pi n} \\ v &= \frac{D_e}{D_i} \end{aligned} \tag{2}$$

Further, the axial component v_a of the absolute velocity and the flow rate Q are obtained with the following formulae:

$$\begin{aligned} v_a &= k_a\sqrt{2gH}, \\ Q &= \frac{\pi(1-v^2)D_i^2 v_a}{4} \end{aligned} \tag{3}$$

Next, dividing the blade into several parts from hub to tip, vortex design is determined. Referencing specific speed n, the number of blades z is determined, and then the pitch t at each radial point φ is calculated by the following equation:

$$t = \frac{\pi D}{z} \tag{4}$$

The velocity triangle of this runner is illustrated in Figure 1 [35] and [36].

The periphery velocity (c) at the inlet and outlet of a blade, which depends on the impeller rotational speed (ω) and the blade radius can be obtained by:

$$C_1 = C_2 = \omega r \tag{5}$$

While the absolute speed of the turbine is determined by the fluid flow rate through the turbine blades, as shown in the equation.

$$v_1 = v_{2s} = \frac{Q}{S} = \frac{Q}{\pi(r_e^2 - r_i^2)} \tag{6}$$

where S is the tubular cross-section area; and r_e, and r_i = tip and hub blade radius between the runner periphery and internal bulb, are determined according to the following equation,

$$tan\alpha_1 = \frac{v_1}{c_1} = \frac{Q}{S}.\frac{1}{\omega r} \quad (7)$$

$$tan\alpha_2 = \frac{v_{2s}}{c_{1+v_{2r}}} = \frac{v_1}{\omega r+v_{21}} \Leftrightarrow \tan\alpha_2 \frac{Q}{S} \quad (8)$$

A vortex formation is visible in the analysis of the flow downstream of the impeller, which depends on the radius of the blade, the flow cross-section, and the discharge, as per the following equation

$$v_{2t} = \frac{k}{r} \Rightarrow k = -\omega r^2 + \frac{Qr}{Stan\ \alpha_2} \quad (9)$$

Based on Equations (7), (8), and (9), the blade model configuration determines the angles for a given rotational speed and leads to optimum performance.

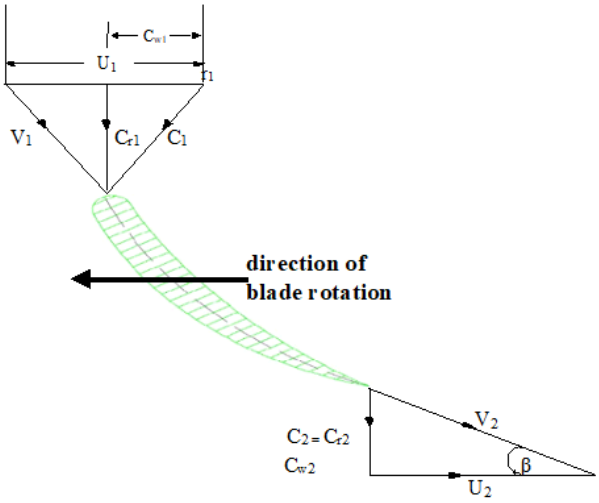

Fig. 1. Inlet and exit velocity triangles at the runner hub.

2.2 Calculation of Turbine Performance

The performance of a water turbine consists of several performance parameters that indicate the characteristics of the turbine, to predict the turbine performances by investigating dimensionless parameters such as water hydraulic power (P_h), tip speed ratio (λ), power coefficient (Cp), and power shaft (P_{shaft}), etc. Some of the factors that affect the water hydraulic power of the propeller turbine such as foil rotor profile, foil arrangement, head, and water discharge, which are theoretically stated as below [11]:

$$P_h = \rho Q g H \quad (10)$$

Where P is the power (watt), ρ is the water density (kg/m^3), g is the gravitational constant (9.81 m/s^2), Q is the discharged (m^3/sec), and H is the gross head (m).

The shaft power is the ability of a turbine to convert water power affected by angular velocity (rpm) and torque (Nm), as shown in the following equation:

$$P_{shaft} = \frac{2\pi nT}{60} \quad (11)$$

Where T is the torque (Nm) and n is the angular velocity (rpm), and T is the mechanical torque (N. m).

The coefficient of power is the amount of water energy that converts the water flow into the generator mechanical energy that passes through the runner blade, which is the ratio between the output power produced by the rotor and the water flow power, as shown in the following equation:

$$C_P = \frac{P_{shaft}}{P_{input}} \quad (12)$$

The tip speed ratio is the ratio of the blade tip speed to the free flow rate. TSR is also a comparison between the power coefficient and the torque coefficient, formulated as follows:

$$\frac{C_P}{C_T} = \frac{\omega R}{v} = \lambda \quad (13)$$

Where λ is the TSR, and ω is the turbine rotational speed (rad/s), R is the radius of the turbine (m).

The specifications detailed the design are displayed in Table 1. In this study, the first step is to make a precise 3D model to determine the fluid flow inside the turbine section. The 3D model of the runner created using the Autodesk Inventor software was exported in the IGES format. Once the 3D solid modelling is developed, all related 3D solid modelling runner blades will be combined with domains by subtracting both of them under Boolean command. In the end, this process will obtain complete geometry files and ready to mesh in the CFD.

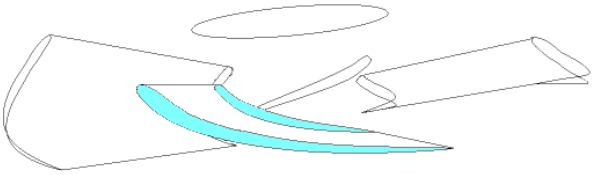

(a)

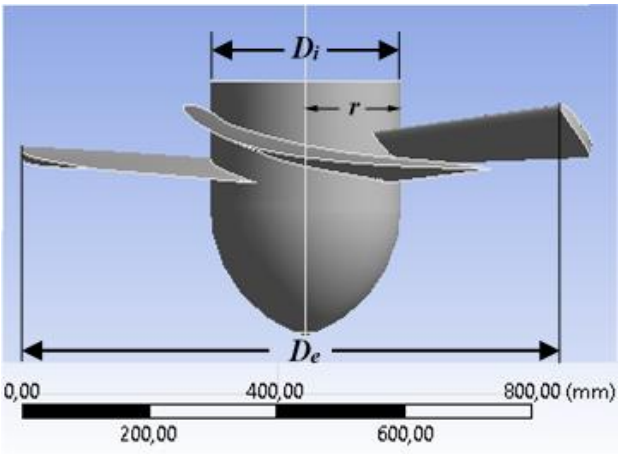

(b)

Fig. 2. (a) Blade geometric profile and (b) 3D Blade geometry model.

From the information in Table 1 and the diameter calculations, the shape of the runner blades and the tilt pitch angles parameter can now be properly defined. The 3D model of the runner blade is furnished in Figure 3.

Table 1. Details of blade design specifications.

Description	Dimension/Value
Number of Blades	4
Tip diameter (m)	0.30
Hub diameter (m)	0.06
Length runner diameter (m)	0.28
Length runner (m)	0.234
Blade angle (deg)	25, 30, and 35

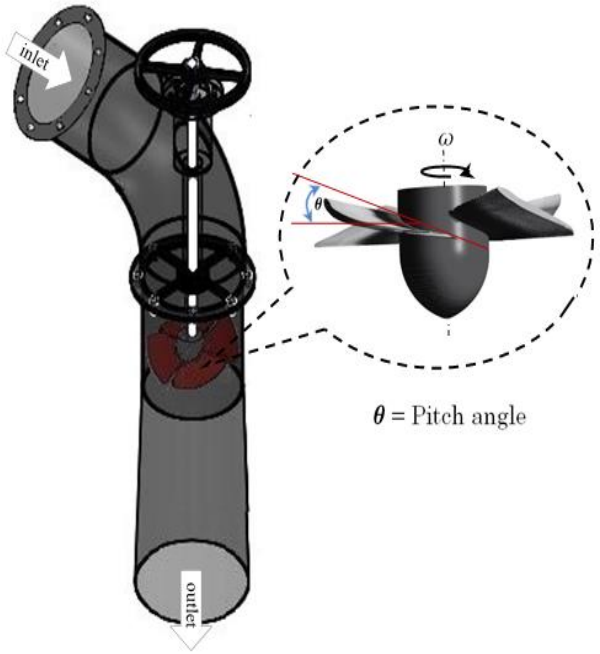

Fig. 3. 3D Runner blade model of the Propeller turbines.

2.3 The k-ω Equation for the Turbulence Model

To analyse the inner flow of the propeller turbine, the Shear Stress Turbulence model has been applied and recommended in this study, because it is not over-predicted in the dissipation rate calculation [37]. The shear stress transport k-ω turbulence model gives a highly accurate onset and amounts of the flow separation under adverse pressure gradients. Hence, the k-ω turbulent model [38] is a model of two common equation used as a cover for the Reynolds averaged Navier Stokes equation (RANS equation). This model tries to predict turbulence using two partial differential equations for the two variables, *k*, and *ω*, with the first variable being the kinetic energy turbulence (*k*) and the second (*ω*) the level of specific dissipation. The eddy v_T viscosity, as required in the RANS equation, is given by $v_T = \frac{k}{\omega}$.. Turbulent kinetic energy *k* and the specifics dissipation rate *ω* are obtained from the following transport equations [39];

k function:

$$:\frac{\partial(\rho k)}{\partial t}+\frac{\partial(u_j k)}{\partial z_j}$$

$$=\rho P-\beta^*\rho\omega k+\frac{\partial}{\partial z_j}\left[\left(\mu+\sigma_k\frac{\rho k}{\omega}\right)\frac{\partial k}{\partial z_j}\right], \quad (14)$$

With, $P=\tau_{ij}\frac{\partial_{U_i}}{\partial_{z_j}}$

ω function:

$$:\frac{\partial(\rho\omega)}{\partial t}+\frac{\partial\left(\rho u_j\omega\right)}{\partial_{z_j}}$$

$$=\frac{\alpha\omega}{k}P-\beta\rho\omega^2+\frac{\partial}{\partial z_j}\left[\left(\mu+\sigma_\omega\frac{\rho k}{\omega}\right)\frac{\partial_\omega}{\partial_{z_j}}\right] \quad (15)$$

$$+\frac{\rho\sigma_d}{\omega}\frac{\partial k}{\partial_{z_j}}\frac{\partial_\omega}{\partial_{z_j}}$$

The turbulence-kinetic-energy equation, which involves the pressure, work diffusion, or dilatation, does not contain the specific compressibility term [40]. In the prediction of flow, separated by shocks, modification of dilatation-dissipation in the k equation also leads to the increase of the compressible mixing-layer, which in turn has a detrimental effect.

The terms turbulent-diffusion in Equations (14) and (15) (σk and $\sigma\omega$) are comparable ($\rho k/\omega$) rather than the eddy viscosity. This means that this specific equation is implicitly affected by the voltage limiter which is a production requirement (via a voltage-Reynolds tensor). As a result, the k-ω model can serve as the foundation of the model with more general prescriptions for calculating Reynolds-voltage tensors, including the algebraic stress model, the full voltage transport model, and even a separate eddy simulation.

2.4 Grid Topology and Generation

The hydrodynamic analysis employs a computational grid that has an automatic ability to produce complicated geometries. Hence, a commercial software Ansys FLUENT is well suited and was utilized for this design problem [41]. For the flow rates considered in microturbines, the maximum thickness of 1mm was taken into account for the blades, due to limitations of the mesh generation. In order to avoid mesh error, the geometry needs to be simplified and cleaned, such as useless point, line and planes. Past researchers have validated the accuracy of numerical simulations using ANSYS Fluent software to solve various fluid flow problems for turbine applications [42], [43], [44], [45].

A resolution study of the grid was carried out to provide insight into the effect of grid distance on the prediction of runner blade performance for propeller turbines. Grid spacing in the blade edge area is crucial for the quality of the mesh produced. This research has used an O-type multi-block unstructured grid (tetrahedral), with node size 219,111 and element

1,223,005. An unstructured grid provides adaptability to complex geometry. The number of layers, which specifies the maximum number of inflation layers, is set as 10 to get a good resolution in the region of interfaces and enhance the results. In the 3D simulation, the cell quality is evaluated as good if the value of the skewness is in the range of 0.25 – 0.5. If the value of the skew is in the range of 0.5-0.75, the quality of the cell is fair (ANSYS, 2017 version 18.2). In this research, the growth rate has been selected as 1.05.

The non-dimensional wall distance (y^+) is a critical parameter for the SST turbulence model. In this study, y^+ less than one was achieved near the solid wall for the blade. The layer thickness impacts the total quality of the mesh. The first layer height (h_0) was chosen as 6.5e-007 m. The edge sizing method was additional grid refinement for the region of interest. The body sizing was used for both rotating and stationary domains. Both edge sizing and body sizing determine the densities of the mesh. In the edge sizing method, number of the division was selected. Following is the skewness value of the mesh for the blade in the range of 0.05-0.7. The average value is about 0.257, and the standard deviation of the skewness around 0.123. According to the relationship between cell skewness and quality, the quality of a mesh can be evaluated as good. The computational domain and meshing on the related blades are shown in Figures 4 (a) and (b).

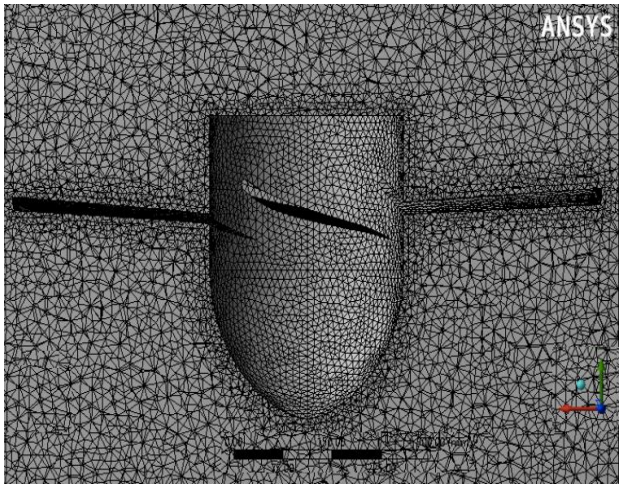

(a)

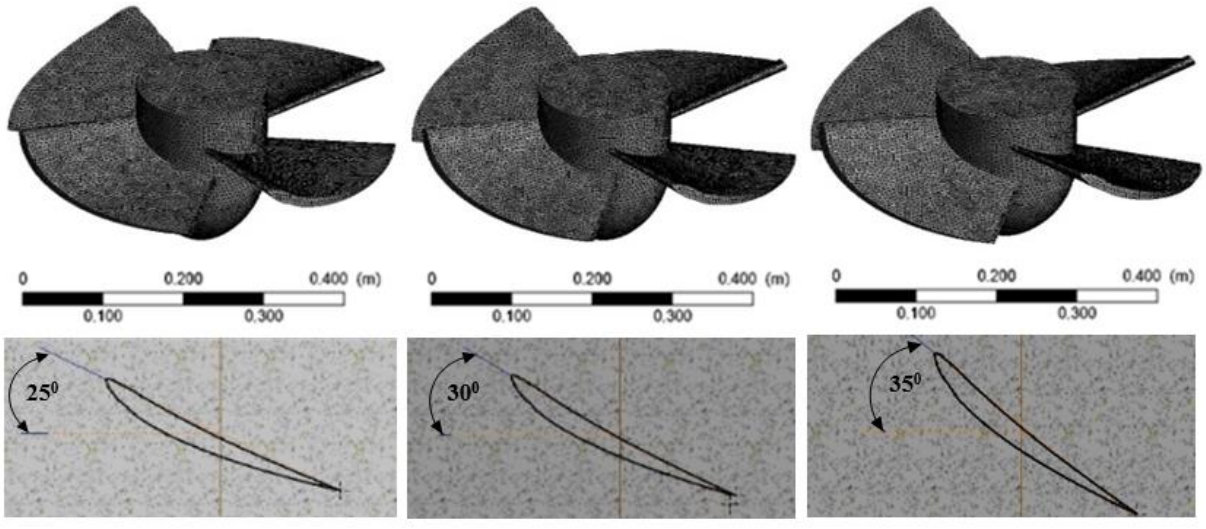

(b)

Fig. 4. (a) Computational domain of blade and (b) Examples of the meshing images, and pitch angle variation details.

2.5 Boundary Condition

Boundary conditions have been specified for the flow variables on the boundaries of the physical model. The four types of boundary conditions (*i.e.*, inlet and outlet pressure, runner, and wall), are a part of the simulation for determining a value of the characteristic variables in the physical limits of the device. On the other hand, the area designated the runners are defined as movable walls, and the rotational speeds around the shaft rotate, which correspond to the center of the runner. On the fields corresponding to the solid surface, the condition of impermeability is imposed to use the standard wall

law for turbulent flow simulations. Thus, the flows of information between these domains will be the grids' interface. As shown in Table 2, the boundary conditions were used for analysis.

2.6 Convergence Test

Convergence tests were performed to ascertain the grid sensitivity of the domain on the solution and to select the least number of iterations. The convergence can be monitored dynamically by checking residuals. The residuals must be kept on decreasing from the start to end of the iterations; in this study, the scaled residuals decrease from 10^{-4} to 10^{-5} for equations. Numerical results have been obtained using about 2021 iterations to obtain a suitable level of solution convergence as shown in Figures 5 a), b), and c) which shows the residual history versus the number of iterations for the grid of 1,223,005 elements.

Table 2. Details of the boundary conditions.

Variable	Value
Material Type	Fluid (water liquid)
Operating Condition	101325 Pa
	Velocity Inlet
	Pressure outlet
Boundary Condition	Stationary and Moving Wall
Interface Domain	Grid Interface
Pressure-Velocity Coupling	SIMPLE
Pressure	Standard
Density [kg/m3]	ρ ¼ 998.2 kg = m^3
Viscosity [kg/m-s]	v ¼ 1.01 × 10−6 m^2 = s

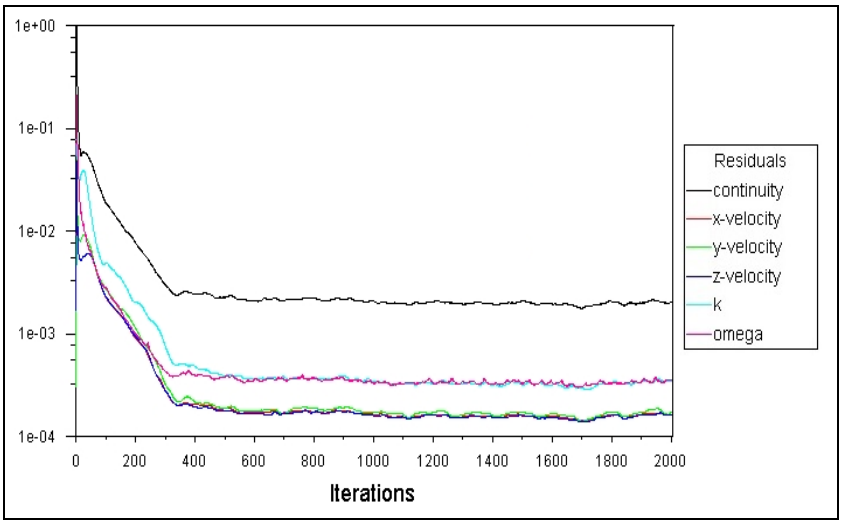

(a) Residual history with the number of iterations on 25 deg

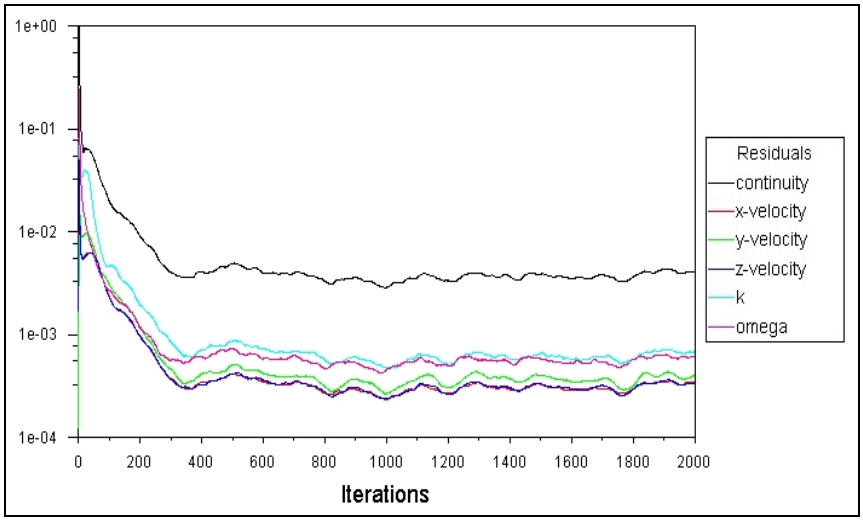

(b) Residual history with the number of iterations on 30 deg

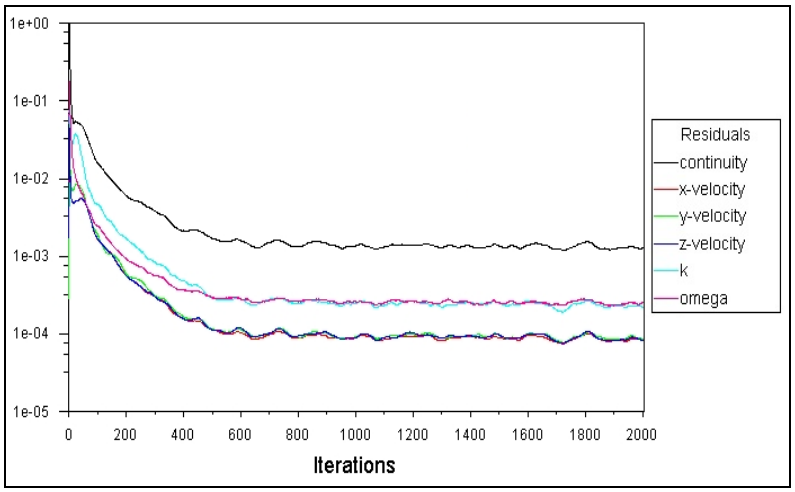

(c) Residual history with the number of iterations on 35 deg.

Fig. 5. Residual history with the number of iterations on 25 - 35 deg.

3. RESULTS AND DISCUSSION

3.1 Pressure Distribution on the Blade Surface

In this work, we had observed that the blade angle affects the pressure distribution that occurs as a result of the blade cross-section. This can be seen from the pressure drop, as the blade angle dimension increases from 25 deg to 30 deg, and continues to decrease as the angle of the blade becomes 35 degrees, and causing the runner's rotation to be lower. The effect of the pressures that occur as a result of this result of the blade cross-section of 35 deg, 30 deg, and 25 degrees is 12.59 Pa, 13.43 Pa, and 13.65 Pa respectively. On the other hand, the increase in flow rate causes the pressure distribution to increase, making the blade rotate faster. Under these conditions, as expected, the rotor functions as a generator (generating energy). However, if the torque produced is opposite to the direction of rotation, the rotor functions as a propeller (converting rotational energy into the flow). In the case of water turbine applications, if the pressure value is too low, then a cavitation phenomenon occurs [44], which can lead to a reduction in the turbine performance. The original data provided with Figures 6 a), b), and c) is illustrative of the high- pressure color map on the cross-section of the blade to each pitch blade angle (a) 25 degrees, (b) 30 degrees, and (c) 35 degrees, and indicates that the stagnation point is the location of the "collision" liquid with the rotor wall. The high pressure in the front of produces a backward force that must be resisted by the thrust-bearing rotor. At the rear of the airfoil, the pressure is low, indicating that the suction area on the blades rotates in the direction of rotation to increase the torque produced.

A discrete mathematical equation (matrix) was used as a calculation for a shear stress distribution on the blade surface for each pitch angle, namely 25 deg, 30 deg, and 35 degrees. Based on the simulation results, the variation in pitch angle affects the shear stress on the blade, but at the same time, it does not indicate a linear increase. Several factors cause these conditions, one of them being a too low flow rate, causing the thrust to decrease. In this research, the magnitude of the shear stress for each pitch angle is known. For a flow rate of 0.2 m^3/s and a pitch angle of 25 deg, 30 deg, and 35 degrees, the respective shear stresses are shown in Figure 7.

3.2 Effect of Pitch Angle to Shear Stresses on the Blade Surface

Figure 8 shows that the shear stress distribution that occurs in the blades causes the amount of friction load due to the viscosity of the fluid flow, which inhibits rotation and decreases the efficiency of the turbine. The shear stress distribution causes the flow concentration to occur in the high-pressure area near the front. Besides, high shear stresses also pose a high risk of abrasion at this location. Hence, it needs to be realized that the full turbulent simulation is not adequate for propeller flows at high load, when laminar and/or transitional boundary layers are prevalent. Based on the simulation, results show that high pressure causes the propeller to expand, thus contributing to the drag and friction coefficient. From Figures 8 a), b), and c), it seems that sizable shear stress occurs at the bottom of the airfoil, because the area has a relatively high velocity. The red color on the tip of the cross-section of the airfoil indicates that a pitch angle of 25 degrees has high shear stress, compared to a pitch angle of 30 degrees and 35 degrees.

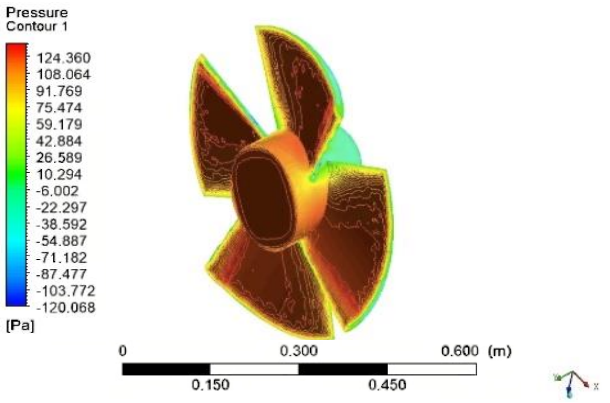

(a) Pressure distribution contour on 25 deg

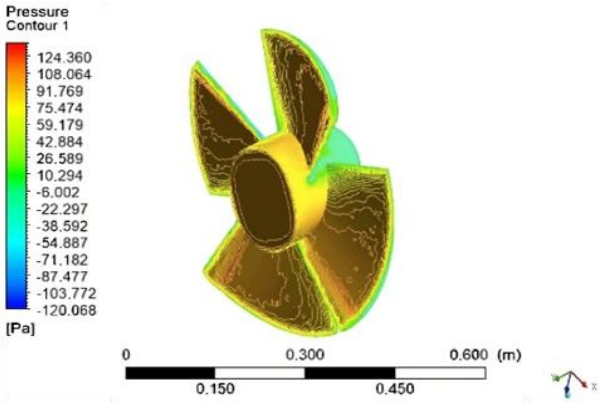

(b) Pressure distribution contour on 30 deg

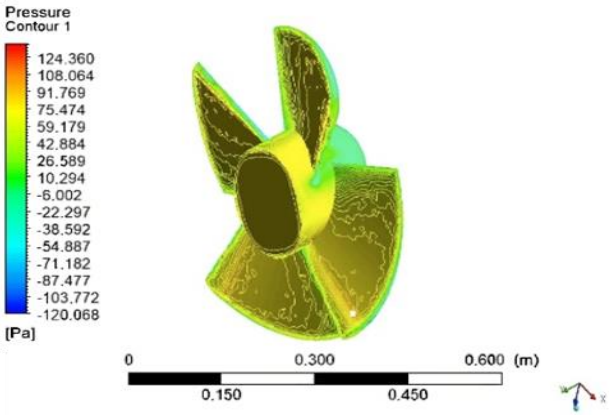

(c) Pressure distribution contour on 35 deg

Fig. 6. Pressure distribution contour on 25 - 35 deg.

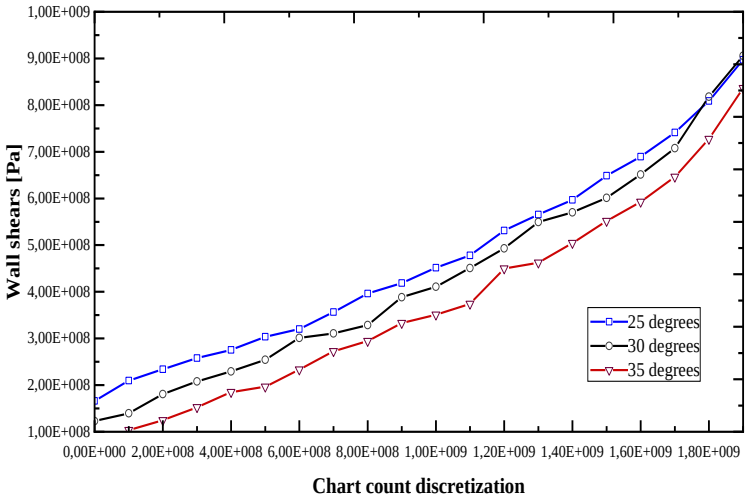

Fig. 7. Wall shears and discretization on different blade angles.

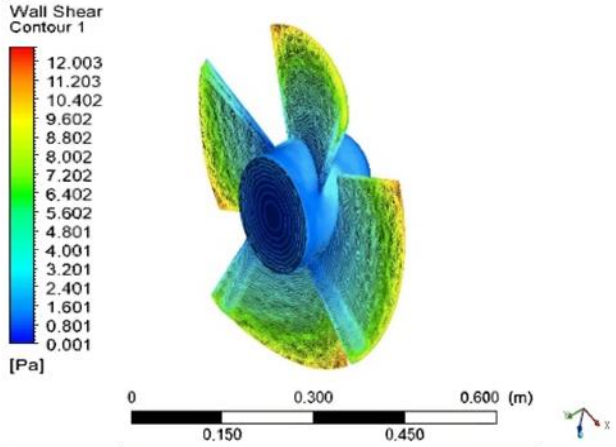

(a) Shear stresses distribution contour on 25 deg

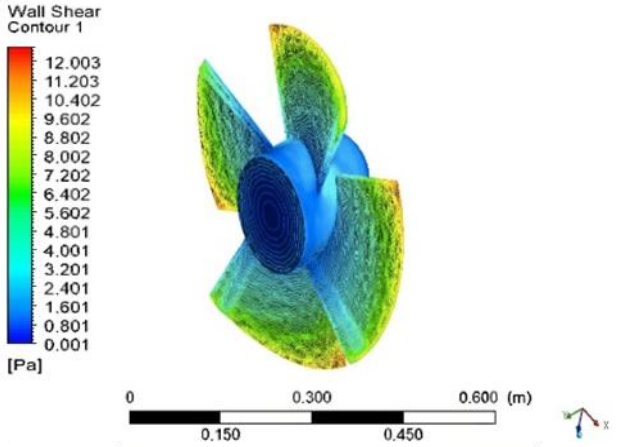

(b) Shear stresses distribution contour on 30 deg

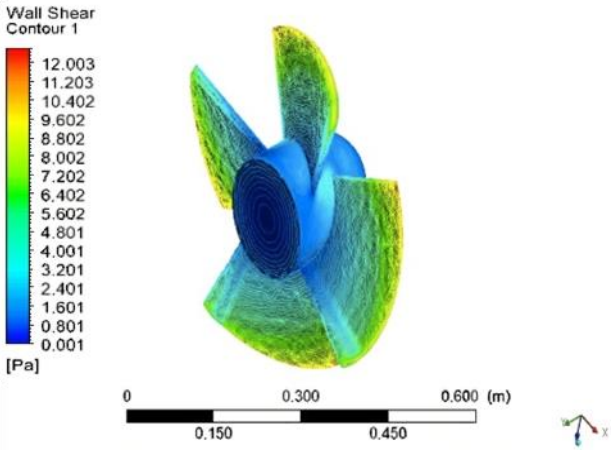

(c) Shear stresses distribution contour on 35 deg

Fig. 8. Shear stresses distribution contour on 25 - 35 deg.

3.3 Streamline Around the Blade

Propellers generate a suction effect, and the flow separation creates a recirculating flow region which is near the hub, as shown in Figures 9a, b), and c). The streamlines that are numerically generated in Figure 9 pass through the inlet and outlet of the rotor for each runner blade change, as the angled spacing increased. The figures indicate that the smaller the pitch angle, the higher the turn that is formed from the flow pattern, and the large the pitch angle, the straighter the flow pattern looks. The analysis of the pitch angle result reveals that at 25 degrees, at flow rate of 0.2 m^3/s, laminar flows can be observed, while for pitch angles of 30 degrees and 35 degrees with the same flow rate, turbulent flow is observed. The turbulence factor in a propeller water turbine is unavoidable and is one of the factors to be taken into consideration in the design of turbines. The blade performance due to the influence of the flow rate is worst with a blade angle of 35 degrees. As shown in Figure. 9c, the flow rate that occurs does not hit the blade cross-section area evenly, thus lowering pressure. In this case, the momentum across the exit plane is relatively large, leading to a low level of total thrust.

Measured power outputs and torque of the runner blades at different flow rates are shown graphically in Figures 10 and 11. The theoretical results were computed using Equations (10), (11), and (12) for each pitch angle under consideration.

Figure 10 shows that the inlet flow rate affects power output due to the distribution of the flow rate and changes in the blade angle. Theoretically, this proves the characteristics of the propeller turbines [46]. Hence, the output power for each pitch angle is based on the flow rate distribution. The value of the computational results shows that the maximum power output is 1357 watts at 950 RPM, obtained at a flow rate of 0.2 m^3/s and an angle of 25 degrees. At the same flow rate, the minimum power output of 112 watts is obtained at an angle of 35 degrees. To further ensure the validation of the CFD methodology, numerical results were compared with the calculating results using the Equation (10). By design parameters (*i.e.*, 1.5 meters head, 0.08 - 0.2 m^3/s discharge), the water density (998 kg/m^3) and the gravitational constant (9.81 m/s^2), it is shown that the theoretical calculation results and the simulation results reveal close comparison beyond the value of 94%, which indicates that the simulation results are reliable. It can be seen from the simulation results in Figure 10 that the average reduction value for each angle is 3.15 watts due to different flow rates resulting from fluid interactions with turbine blades.

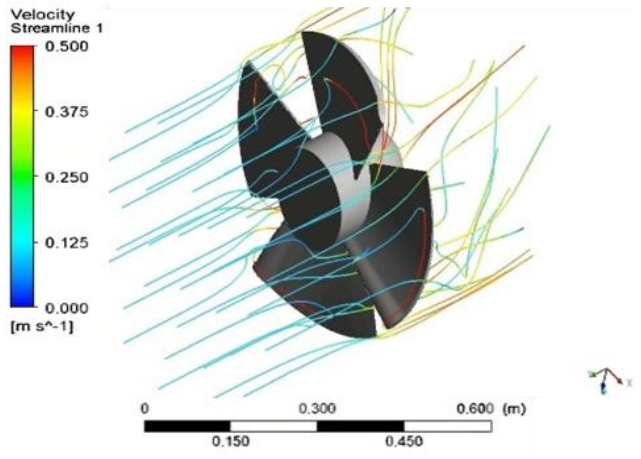

(a) Streamlines and velocity contour on 25 deg

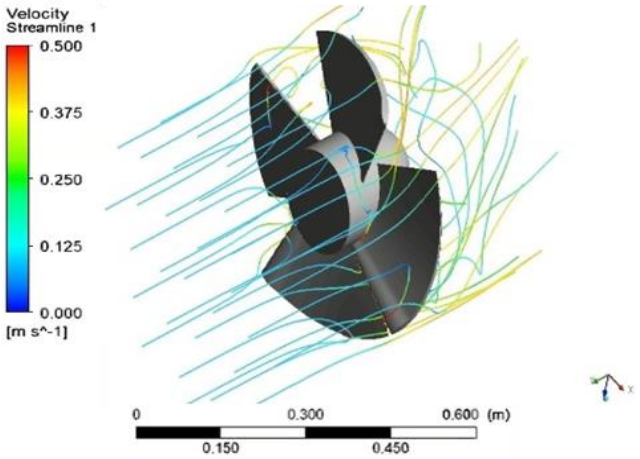

(b) Streamlines and velocity contour on 30 deg

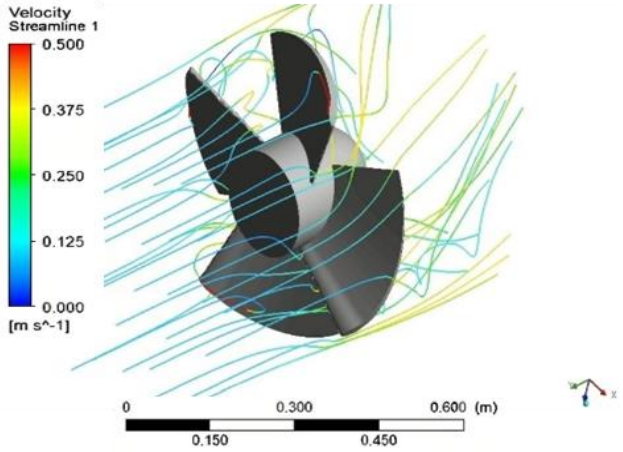

(c) Streamlines and velocity contour on 35 deg

Fig. 9. Streamlines and velocity contour on 25 - 35 deg.

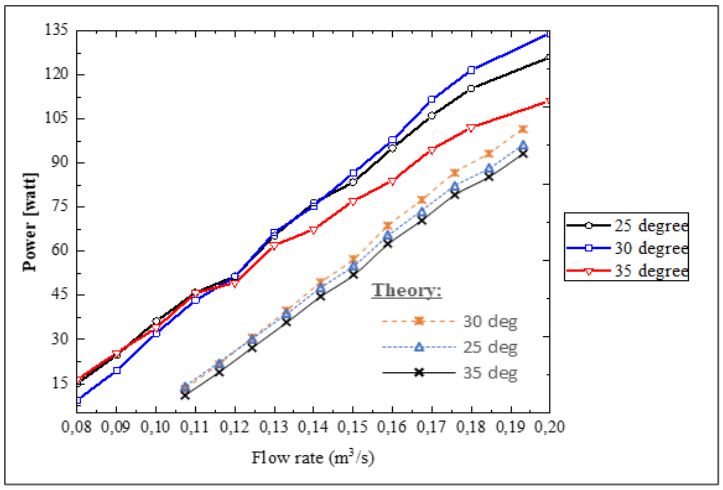

Fig. 10. Power curves on the various flow rate.

The effect of the flow rate distribution on the torque is shown in Figure 11. The analyzed results reveal that the value torque increased monotonically with the rise of the flow rate. However, when the rotational speed increased to a specific value, the value torque began to decrease. In the low flow rate, the torque value decreased with the pressure drop difference and improved with the rise of the flow rate. Based on calculations using Equation (11), the lowest torque values are obtained from the pitch angle of 35 degrees at a minimum flow rate of 0.08 m^3/s and the maximum torque value at an angle of 25 degrees with an entrance flow rate of 0.2 m^3/s. However, when the flow rate increases by an average of 0.14 m^3/s at an angle of 25 degrees, the torque value reaches 3.12 Nm. With the same flow rate and with an increase in angles to 30 degrees and 35 degrees, the torque value reaches 2.91 Nm and 2.74 Nm, respectively. The analysis results of

various blade angles show a reduction of 0.2 Nm in the average torque value. It is known from these studies that the increase in the torque value is due to the increased flow rate from 0.08 up to 0.2 m^3/s, and also due to the narrowing effect of the blade angle from 35 deg to 30 deg and 25 deg. Further, the data is validated by comparing the summation value based on a theory with the CFD data results, which is represented graphically in Figure 11. From a comparison of the results, it is evident that the CFD data are sufficiently in agreement with theoretically valued results.

The relationship of *Cp* to flow rate is illustrated in Figure 12. Based on the calculations using Equation (12), for a pitch angle of 25 degrees at a minimum flow rate of 0.08 m^3/s, the *Cp* result is 74.64. When the angle is increased to 30 degrees at the same flow rate, the *Cp* obtained is 69.16. At a pitch angle of 35 degrees at the same flow rate, the result obtained is 65.68. The simulation results lead to the conclusion that with increasing pitch angle, the output power generated by the turbine blades' runner speed is affected by the flow rate. The higher the angle, the lower the flow rate of the small output power. However, it will be different if the pitch angle is reduced, and the turbine output power becomes higher. Figure 13 shows in a graph the effects of the blade angles on runner blade performance. Based on the calculation result using Equation (13), the pitch angle of 25 degrees with a maximum flow rate of 0.2 m^3/s the value obtained is 28.26, and at a 30 degrees pitch angle at the same speed, the value is 26.99. However, with a pitch angle of 35 degrees and a flow rate of 0.08 m^3/s, the result is 25.80. It seems that the 25 degrees pitch angle yields the best performance compared to the blade angles of 30 degrees and 35 degrees. However, turbine blades with angles of 30 degrees tend to perform better than the ones with a 35-degree angle, though both have peak values of power coefficient adrift of difference 1.2.

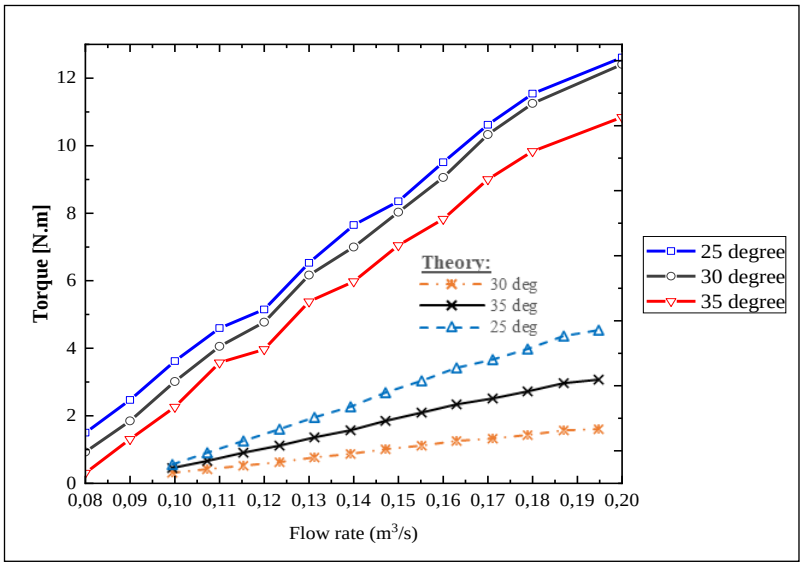

Fig. 11. Power curves on the various flow rate.

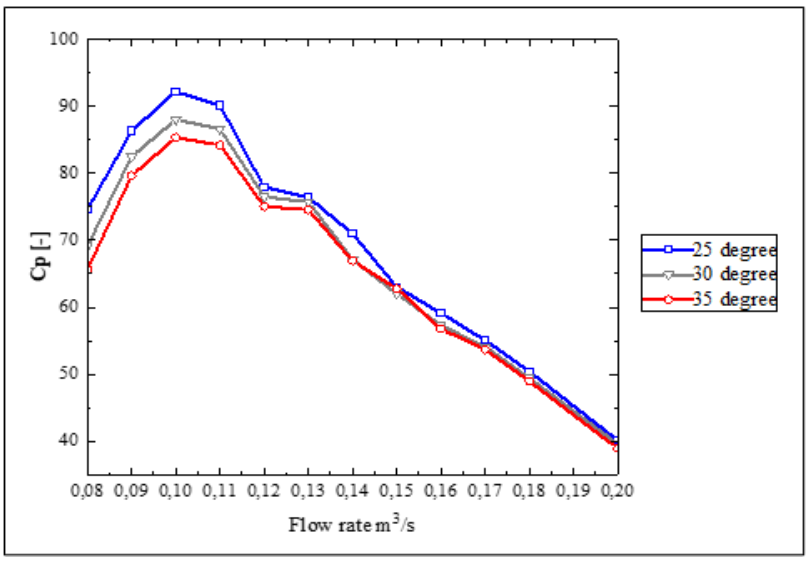

Fig. 12. Power coefficient curves on the various flow rate.

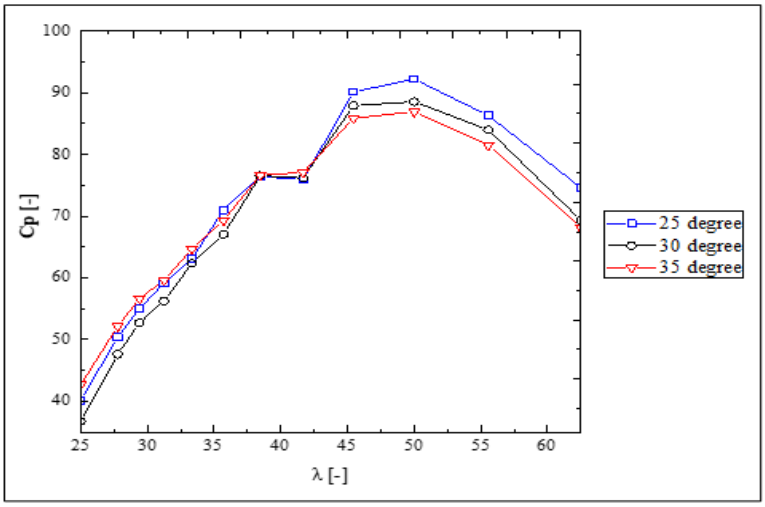

Fig. 13. Power coefficient (C_p) versus TSR (λ).

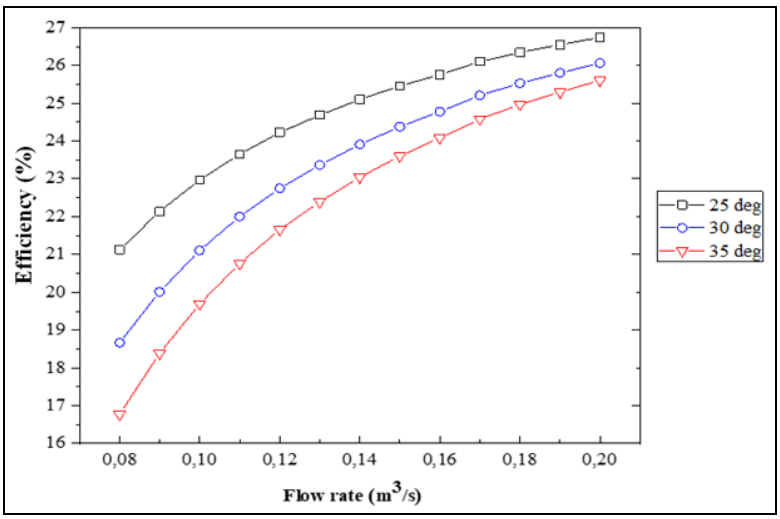

Fig. 14. Efficiency curves on the various flow rate.

3.4 Model Validation

After CFD analysis, it becomes very important to validate the results achieved by comparing CFD results with available experimental data [47]. On the analysis result, the inlet flow rate affects power output, to the case where there is no significant increase in power due to the distribution of the flow rate to changes in angle. Theoretically, these prove the characteristics of the hydro-propeller turbine [48]. To future ensure the validation of CFD methodology, the results of the numerical simulations were compared with experimental results [48], [49], and [50], where varied blade profiles can affect the value of efficiency and can increase the power output of the propeller turbine. This is associated with a decrease in flow rate which causes a lower power output with an average reduction value for each corner of 3.15 watts. These results are similar to those of the studies for the hydro tubular propeller [20] but provide different answers compared to the reviews [51], based on angles of 20 degrees and 30-degrees for better results. Of all the variations in blade angles in this study, it is known that a 25-degree pitch angle at a flow rate of 0.2 m^3/s has the best performance, compared to a power output of 1357 watts with an efficiency of 26.74% at 950 RPM. These results are different from those obtained by previous researchers for the same type of turbine [22], particularly those of [52], which found that the highest yield on the use of the large discharge was 33 degrees with a power output of 17.2 watts at 1283 RPM shaft rotation, the performance coefficient obtained reaching 54%.

4. CONCLUSION

CFD has been used as a tool for analyzing the pressure distribution, shear stresses, and streamlines that pass through the pitch angle of the inlet and outlet of the rotor between the runner blades. The flow rate data for each blade parameter involved was also obtained from this particular analysis. Then the model was validated by comparing the research data to power output calculation and the data of previous researchers. Based on the analysis results, the blade angle, geometric shape, and flow rate affect the performance of the turbines, and the smaller the blade angle, the higher the power output, other than the power coefficient tending to decrease with increasing blade angle and increasing proportionally to the increasing flow rate. The other result is that the surface tension distribution of the airfoil is relatively

higher than that of the rear, because the airfoil geometry is curved, and the pitch angle effect is not zero. The final result of the analysis shows that the power and efficiency coefficients were higher for the blade angle of 25 degrees than for 30 degrees and 35 degrees. However, both correspond to the value of the peak power coefficient. Therefore, further investigation and evaluation through experiments with these blade models are very important.

ACKNOWLEDGEMENT

The author is especially grateful to The Domestic Postgraduate Education Scholarship – Research, Technology, and Higher Education of The Republic of Indonesia (BPPDN – RISTEKDIKTI), Teuku Umar University, and Diponegoro University for financial assistance and opportunities to study and conduct research.

NOMENCLATURE

Symbol	Description	Unit
A	cross-sectional area	m^2
c	absolute velocity	m/s
C_P	power coefficient	
C_T	torque coefficient	
D_e	runner diameter	m
D_i	hub diameter	m
k	turbulence kinetic energy per unit mass	m^2/s^2
p	pressure on the blade surface	Pa
P_{in}	water hydraulic power	Watt
P_{shaft}	power shaft	
Q	flowrate	m^3/s
r	blade radius. Subscript *e* for tip and subscript *i* for hub	m
R	radius of turbine	m
S	tubular cross section area	m^2
T	torque	N.m
u	circumferential velocity	m/s
v	flow velocity. Subscript 1 and 2 for the inlet and outlet of the blade	m/s
w	relative velocity	m/s

Greek Letters

α,	absolute flow angel	°
β	relative flow of blade angel	°
λ	tip speed ratio	
μ	molecular (dynamic) viscosity	kg(m/s)
η	efficiency	%
ρ	mass density of water	kg/m^3
τ	stress	
τ_{ij}	Favre - averaged specific Reynolds-stress tensor	
σ_k	turbulence constant model for the *k* equation	1.0
σ_ω	*k-ω* turbulence constant model	1.3
φ	discharge number	
ω	rotational speed	rad/s
θ	pitch blade angle	°

REFERENCES

[1] Kaygusuz K, 2002. Sustainable development of hydropower and biomass energy in Turkey. *Energy Conversion and Management* 43(8): 1099-1120. doi.org/10.1016/S0196-8904(01)00086-3.

[2] Date A. and A. Akbarzadeh. 2009. Design and cost analysis of low head simple reaction hydro turbine for remote area power supply. *Renewable Energy* 34(2): 409-415. https://doi.org/10.1016/j.renene.2008.05.012.

[3] IEA, 2010. Renewable energy essentials: Hydropower. Retrieved from the World Wide Web. https://www.hydropower.org.

[4] REN21, 2019. Renewbles in cities – 2019 Global status report. Retrieved December 2020 from the World Wide Web: https://wedocs.unep.org/bitstream/handle/20.500.11822/28496/REN2019.pdf.

[5] IEA, 2013. World energy outlook. In *IEA Publications, 9 rue de la Fédération, 75739 Paris Cedex 15 (Second Edition).* Retrieved from the World Wide Web: https://doi.org/10.1111/j.1468-0319.1988.tb00400.x.

[6] Tasri A. and A. Susilawati. 2014. Selection among renewable energy alternative based on a fuzzy analytic hierarchy process in Indonesia. *Sustainable Energy Technology and Assessments*, 7, 34-44. doi.org/10.1016/j.seta.2014.02.008.

[7] ESDM, 2017b. Handbook of energy and economic statistic of Indonesia. Retrieved from the World Wide Web: https://www.esdm.go.id.

[8] Delucchi M.A., and M.Z. Jacobson. 2010. Providing all global energy with wind, water, and solar power, part II: Reliability, systen and transmission cost, and policies. *Energy Policy* 39(3): 1170-1190. doi.org/10.1016/j.enpol.2010.11.045.

[9] REN21, 2017. Renewables: Global status report. In *Renewable and Sustainable Energy Reviews*. Retrieved November, 27 2020 from the World Wide Web: https://doi.org/10.1016/j.rser.2016.09.082.

[10] Purwanto W.W., Nugroho Y.S., Dalimi S., Soepardjo H., Wahid A., Supramono D., Herminna D. and T.A. Adilina, 2006. Indonesian outlook and statistic. *University of Indonesia Assessment*. Retrived from the World Wide Web: https://doi.org/10.13140/RG.2.1.1798.4080.

[11] ESHA, 2004. Guide on how to develop a small hydropower plant : 154-196. Retrieved from the World Wide Web: https://energypedia.info.

[12] Okot D.K., 2013. Review of small hydropower technology. *Renewable and Sustainable Energy Reviews* 26: 515-520. doi.org/10.1016/j.rser.2013.05.006.

[13] Ramos H.M., Borga A. and Simão M., 2009. New design solutions for low-power energy production in water pipe systems. *Water Science and Engineering* 2(4): 69-84. doi.org/10.3882/j.issn.1674.2009.04.007.

[14] Pribadyo P., Hadiyanto H., and Jamari J., 2019. Study of low head turbine propellers axial flow for use of Micro-hydropower Plant (MHP) in Aceh, Indonesia. *Journal of Physics: Conference Series* 1524*(1)*. Retrieved from the World Wide Web: https://doi.org/10.1088/1742-6596/1524/1/012019.

[15] Laghari J.A., Mokhlis H., Bakar A.H.A. and Mohammad H., 2013. A comprehensive overview of new design in the hydraulic, electrical equipment, and controllers of mini hydro power plants making it cost-effective technology. *Renewable and Sustainable Energy Reviews* 20: 279-293. Retrieved from the World Wide Web: doi.org/10.1016/j.rser.2012.12.002.

[16] Ghadimi A.A., Razavi F. and Mohammadian B. 2011. Determining optimum location and capacity for micro hydropower plants in Lorestan Province in Iran. *Renewable and Sustainable Energy Reviews* 15(8): 4125-4131. doi.org/10.1016/j.rser.2011.07.003.

[17] Roque A., Sousa D.M., Casimiro C. and Margato E., 2010. Technical and economic analysis of a micro hydro plant - A case study. In *International Conference on The European Energy Market (EEM 2010)*. Retrieved from the World Wide Web: doi.org/10.1109/EEM.2010.5558735.

[18] Saghir J., 2005. Energy and poverty: Myths, link, and policy issue. Retrieved November 29, 2020 from the World Wide Web: https://documents1.worldbank.org/curated/en/544511468313733634/pdf/374810Energy0WorkingNotes1401PUBLIC1.pdf.

[19] Dixon S.L., 1998. Fluid mechanics. *Thermodynamics of Turbomachinery* (4thed.) 23(3).

[20] Ramos H.M., Simão M. and Kenov K.N, 2012. Low-head energy conversion: A conceptual design and laboratory investigation of microtubular hydro propeller. *ISRN Mechanical Engineering 2012* : 1-10. https://doi.org/10.5402/2012/84206.

[21] Wang X. and K. Walters, 2012. Computational analysis of marine-propeller performance using transition-sensitive turbulence modeling. *Journal of Fluids Engineering, Transactions of the ASME* 134(7): 1-10. doi.org/10.1115/1.4005729.

[22] Othman M.M., Razak A.J., Bashar M.F., Muhammad N.S., and Sopian K., 2014. CFD Analysis on the flat runner blades of propeller's turbine under low head and low flow condition. *Applied Mechanics and Materials.* 699: 437-442. https://doi.org/10.4028/www.scientific.net/amm.699.437.

[23] Nuantong W. and S. Taechajedcadarungsri. 2009. Flow simulations on blades of hydro turbine. *International Journal of Renewable Energy 4*(2): 0–5.

[24] Byeon S. and Y. Kim. 2013. Influence of blade number on the flow characteristics in the vertical axis propeller hydro turbine. *International Journal of Fluid Machinery and Systems* 6(3): 144-151. https://doi.org/10.5293/IJFMS.2013.6.3.144.

[25] Zhou D., Gui J., Daniel Z., Chen H., Yu Y. and Yu A, 2019. Development of an ultra-low head Siphon hydro turbine using computational fluid dynamics 181: 43-50. *Energy*. https://doi.org/10.1016/j.energy.2019.05.060.

[26] Simpson R. and A. Williams. 2006. Application of computational fluid dynamics to the design of pico propeller turbines. *Proceedings of The International Conference on Renewable Energy for Developing Countries*. Retrieved from the World Wide Web: https://files.udc.edu/docs/cere/ICREDC06paper_simpson.pdf.

[27] Trivedi C., Cervantes M.J., and Dahlhaug O.G., 2016. Numerical techniques applied to hydraulic turbines: A perspective review. *Applied Mechanics Reviews* 68(1): 1-18. doi.org/10.1115/1.4032681.

[28] Shukla R.S. and C. Parashar, 2017. Design of propeller turbine for micro hydropower station using CFD. *International Journal of Scientific Engineering and Science* 1(7): 37-41. Retrieved December 10, 2020 from the World Wide Web: http://ijses.com/.

[29] Oo L.L., Win S.Y., and Lin K.Z., 2018. Design of blade for 5 kW propeller turbine. *International Journal of Science and Engineering Applications 7*(10): 336-340. Retrieved from the World Wide Web: https://doi.org/10.7753/ijsea0710.1002.

[30] Nishi Y., Kobayashi Y., Inagaki T., and Kikuchi N., 2016. The design method of axial flow runners focusing on axial flow velocity uniformization and its application to an ultra-small axial flow hydraulic turbine. *International Journal of Rotating Machinery*. Retrieved from the World Wide Web: https://doi.org/10.1155/2016/5390360.

[31] Djodikusumo I., Diasta I.N., and Koeshardono F., 2016. The modeling of a propeller turbine runner in 3D solid using 3D equation curve in Autodesk Inventor 2015. *Applied Mechanics and Materials* 842(Table 1): 147-163. https://doi.org/10.4028/www.scientific.net/AMM.842.147.

[32] Singh P. and F. Nestmann. 2009. Experimental optimization of a free vortex propeller runner for micro hydro application. *Experimental Thermal and Fluid Science* 33(6): 991-1002. doi.org/10.1016/j.expthermflusci.2009.04.007.

[33] Adhikari P., Budhathoki U., Timilsina S.R., Manandhar S. and Bajracharya T.R., 2014. A study on developing pico propeller turbine for low head micro hydropower plants in Nepal. *Journal of the Institute of Engineering* 9(1): 36-53. doi.org/10.3126/jie.v9i1.10669.

[34] Wardhana E.M., Santoso A., and Ramdani A.R., 2019. Analysis of Gottingen 428 airfoil turbine Propeller Design with Computational Fluid dynamics method on gravitational water vortex power plant. *International Journal of Marine Engineering Innovation and Research* 3(3). doi.org/10.12926/j25481479.v313.4864.

[35] Dixon S.L., 1998. Fluid Mechanics, *Thermodynamics of Turbomachinery* (4th ed.) 23(3), Chapters 2, 6 and 9.

[36] Gorla R.S.R. and A.A. Khan. 2003. Turbomachinery Design and Theory (1st ed.). Marcel Dekker, Inc., New York, U.S.A.

[37] Syahputra M.F. and D. Adanta. 2020. Study of turbulence model for performance and flow field prediction of pico hydro types propeller turbine 8(8): 26-34.

[38] Menter F.R., 1994. Two-equation eddy-viscosity turbulence models for engineering applications. *AIAA Journal* 32(8): 1598-1605. doi.org/10.2514/3.12149.

[39] Wilcox D.C., 2008. Formulation of the k-ω Turbulence Model Revisited. *AIAA Journal*. 46(11): 2823-2838. doi.org/10.2514/1.36541.

[40] Robinson D.F. and H.A. Hasan, 1996. A two-equation turbulence closure model for wall bounded and shear flows. *Fluid Dynamics Conference* : 1-11. doi.org/10.2514/3.13785.

[41] ANSYS, 1., *ANSYS CFX-Solver Theory Guide.* 2009. Cononsburg P.A.

[42] Prasad V., 2012. Numerical simulation for flow characteristic of axial flow hydraulic turbine runner. *Energy Procedia* 14(2011): 2060-2065. doi.org/10.1016/j.egypro.2011.12.1208.

[43] Singh P. and F. Nestmann. 2010. Exit blade geometry and part-load performance of small axial flow propeller turbines: An experimental investigation. *Experimental Thermal and Fluid Science* 34(6): 798-811. doi.org/10.1016/j.expthermflusci.2010.01.009.

[44] Kumar P. and R.P. Saini. 2010. Study of cavitation in hydro turbines- A review. *Renewable and Sustainable Energy Review* 14(1): 274-383. doi.org/10.1016/j.rser.2009.07.024.

[45] Adanta D. Fattah M.R., and Nura M.M., 2020. Comparasion of standard k-ε and SST k-ω turbulence model for turbulence models. *Journal of Mechanical Science and Engineering* 7(2): 39–44.

[46] Celso P. and I. de Minas. 1998. Layman's handbook on how to develop a small hydro sites (2nd ed). European Commission: Belgia: 179-183.

[47] Pelletier D., 2015. Verfication, validation, and uncertainty in computational fluid dynamics. Retrieved October 1 from the World Wide Web: https://doi.org/10.1139/L10-032.

[48] Shantika T., Putra A., and Obaja R.K., 2016. Pico hydro 100Watt portable flow simulation on 2 meters head. In *Proceedings of the National Seminar on Application of Science & Technology* (SNAST): 491-497.

[49] Ramos H.M., Simao M., and Borga A., 2013. Experiments and CFD analyses for a new reaction microhydro propeller with five blades. *Journal Energy* 139: 109-117.

[50] Singh P. and F. Netsmann. 2012. Influence of the blade hub geometry on the performance of low-head axial flow turbines. *Journal of Energy Engineering* 138: 109-118.

[51] Chelabi M.A., Hamidou M.K., and Hamel M., 2017. Effects of cone angle and inlet blade angle on mixed inflow turbine performances. *Periodica Polytechnica Mechanical Engineering* 61: 225-233.

[52] Bisri H., Himawanto D.A. and Tjahyana D.D.D.P., 2020. The Influence of inlet hub angle on propeller turbine in horizontal flow 10(2): 88-94. https://doi.org/10.29303/dtm.v10i2.345.

[53] ANSYS. *ANSYS FLUENT Theory Guide*, 2017, Canonsburg, P.A.